IMAGINE: the Neutron Protein Crystallography Beamline at the High Flux Isotope Reactor

Flora Meilleur[a,b*], Andrey Kovalevsky[a], Dean A. A. Myles[a]

[a]Neutron Scattering Division, Oak Ridge National Laboratory, Oak Ridge, TN 37831

[b]Department of Molecular and Structural Biochemistry, North Carolina State University, Raleigh, NC 27695

*Corresponding author: meilleurf@ornl.gov

Keyword: neutron, crystallography, polychromatic, hydrogen, deuterium, enzyme, protonation, water

Abstract

IMAGINE is a high intensity, quasi-Laue neutron crystallography beamline developed at the 85 MW High Flux Isotope Reactor (HFIR) at Oak Ridge National Laboratory (ORNL). This state-of-the-art facility for neutron-diffraction enables neutron protein structures to be determined at or near atomic resolutions from crystals with volumes of less than 1 mm^3 and unit cell edge of less than 150 Å. Beamline features include elliptical focusing mirrors that deliver neutrons into a 2.0 × 3.2 mm^2 focal spot at the sample position, and variable short and long wavelength cutoff optics that provide automated exchange between multiple wavelength configurations. The beamline is equipped with a single-axis goniometer, neutron-sensitive cylindrical image plate detector and room temperature and cryogenic sample environments. This article describes the beamline components, the diffractometer and the data collection and data analysis protocols that are used, and outlines the protein deuteration, crystallization and conventional crystallography capabilities that are available to users at ORNL's neutron facilities. We also present examples of the scientific questions being addressed at this beamline and highlight important findings in enzyme chemistry that have been made possible by IMAGINE.

1. Introduction

Neutron crystallography is an inherently flux-limited technique. Available neutron fluxes are several orders of magnitude less than the X-ray flux available from modern in-house generators and synchrotrons. This limitation is the primary motivation for increasing the scattering power of the protein crystal through the isotopic labeling and crystal growth techniques discussed in the previous sections (Devos et al., this issue; Fisher et al., this issue). Low available flux also results in the long exposure times required to measure a neutron diffraction dataset to sufficient resolution and completeness. While complete X-ray datasets can be measured in seconds or less at high-intensity X-ray sources, neutron datasets typically require days to weeks for collection. However, through recent advances in instrumentation and labeling it has become possible, in special cases, to obtain useful neutron datasets in a single day or less .

Instruments can be divided into three groups based upon mode of operation, namely monochromatic (Schrader et al., this issue; Forsyth et al., this issue), quasi-Laue (also known as "pink-Laue") (Blakeley et al., this issue; Coquelle et al., this issue; and IMAGINE presented here) and time-of-flight (TOF) Laue (Coates, this issue; Tanaka, this issue; Oksanen, this issue) modes. All instrument detector systems are designed to maximize coverage of reciprocal space so that a large number of stimulated reflections that can be recorded simultaneously whether the instrument uses mono- or polychromatic incident radiation. Typically, neutron protein crystallography beam lines take advantage of longer wavelength neutrons to maximize the intensities of the diffraction peaks which are proportional to the square on the incident wavelength, as shown in Equation (1), and to reduce spatial overlap according to Bragg's law ($2d*\sin(\lambda)= \lambda$). At the wavelength typically used for X-ray crystallography ($\lambda \leq 1.54$ Å), the diffracted beams lie on cones in the forward scattering direction, and two-dimensional detectors are installed downstream of the crystal. At the longer wavelengths (2.3 Å $< \lambda <$ 6.0 Å) used by cold-neutron diffractometers, the high resolution diffraction also occurs in the backscattering direction. Instrument detector arrays approximate cylindrical or spherical geometries to record both forward- and backscattering reflections.

$$\langle I \rangle \propto \frac{I_0 \times |F|^2 \times V \times \lambda^2}{v_0^2} \quad (1)$$

The IMAGINE beam line takes advantage of the high time-integrated neutron flux provided by the steady-state operation of a reactor to greatly increases the number of stimulated reflections at each crystal setting relative to monochromatic mode {Meilleur, 2013 #889;Schroder, 2018 #1227}. The broad wavelength bandpass therefore is an effective use of neutrons available from the reactor source, and the configuration avoids the need for a monochromator crystal upstream of the sample. Quasi-Laue represents a compromise on the amount of observed incoherent background with it being more than that observed with monochromatic radiation but less than that observed with truly "white-beam" radiation {Meilleur, 2006 #280}. While the monochromatic geometry produces data sets of higher quality compared to the quasi-Laue geometry (either for X-rays or neutrons) for neutron protein crystallography the quasi-Laue configuration has the unique advantage of allowing smaller crystals and/or shorter exposure times to be used {Helliwell, 1997 #1132}.

2. Beam line overview

2.1. Neutron source

Oak Ridge National Laboratory (Oak Ridge, TN, USA) operates two powerful neutron sources for neutron scattering research, the Spallation Neutron Source (SNS), which currently provides

the most intense pulsed neutron beams in the world, and the 85 MW High Flux Isotope Reactor (HFIR), which currently provides one of the highest steady-state neutron fluxes in the world. The HFIR is equipped with a high-performance cold neutron source that has a brightness of 1.6×10^{13} n/cm^2·s·ster·Å at the peak (λ=2.6 Å) and delivers neutrons to a suite of instruments that are optimized for structural biology and materials research {Lynn, 2006 #186;Wignall, 2012 #465}{Crow, 2011 #486}{Heller, 2014 #1346}

2.2. Beamline optics

The instrument sits on the end-station of cold guide number 4 (CG-4), which has a flux of $2x10^9$ n s^{-1} cm^{-2} over the useful 2-10 Å wavelength range. The instrument receives neutrons from a 19 x 12mm^2 section of CG-4. The neutron wavelength and bandpass delivered to the sample is varied by automated exchange of 3 neutron flat mirrors and 3 pairs of neutron filters that provide short wavelength (λ_{min}=2.0, 2.8 and 3.3 Å) and long wavelength (λ_{max}= 3.0, 4.0 and 4.5 Å) cut-offs, respectively. A pair of elliptically shaped mirrors then collects and focuses the resulting beam vertically and horizontally down to 2x3.2 mm^2 at the sample position, with full width vertical and horizontal divergence of 0.5° and 0.6°, respectively. This results in a more than 20-fold increase in flux density at the sample position.

2.3. Diffractometer

The diffractometer uses a cylindrical neutron image plate design {Niimura, 1994 #1360}{Cipriani, 1996 #1364}. The diffractometer is available commercially from ARINAX, France (Fig. 1). The detector system has a broad dynamic range (>10,000), high spatial resolution (250 µm), and high detective quantum efficiency (DQE) of 47% for the standard 2.8–4.5 Å quasi-Laue configuration.

A B 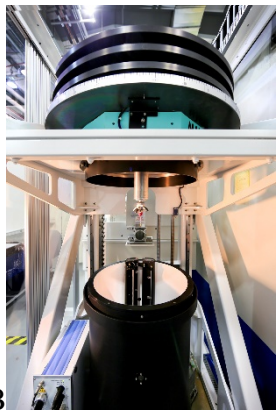

Figure 1: IMAGINE installed on CG-4D. A. IMAGINE is installed in a 4”-thick steel wall enclosure next to the Bio-SANS instrument. The elliptical mirror chamber sits directly upstream of the instrument. B. The image plate detector is mounted inside a cylindrical drum with the radius of 200 mm. The erasing and reading system is placed in the backscattering position.

Crystals are mounted on a sample stick with automated φ-axis rotation for room temperature data collection. (Photo credit: Jason Richards, ORNL)

2.4. Data collection and reduction

The flats mirrors and filters are remotely controlled through their respective controllers and software. Data acquisition is controlled through a graphical user interface (GUI) developed the manufacturer of the diffractometer, ARINAX. IMAGINE is currently equipped with a single-axis goniometer. Data collection at two or more κ angles is essential when using longer wavelength radiation because the curvature of the Ewald sphere is such that the blind region is significant at any one κ setting. In addition, instruments using a cylindrical detector geometry (BIODIFF, IMAGINE, and LADI-III) have large, systematic vacancies in their coverage of reciprocal space along the cylindrical long axis. Reflections absent due to detector coverage can be recovered by using more than one κ angle.

Cold neutrons (< 50 meV) do not induce ionization in biological samples. Therefore, cryogenic sample temperatures are not necessary to protect against radiation damage in the protein crystal, and the majority of experiments are performed at ambient temperature. For room temperature data collection crystals are mounted in quartz capillaries. While room temperature data collection is typical, cryo-crystallography does, however, reduce thermal disorder in protein crystals and makes possible the study of reaction intermediates and temperature sensitive systems {Myles, 2012 #1365}. For either temperature condition, crystal mounting and alignment on the goniometer are performed manually. Given that data collection time exceeds days, manual centering is not a significant overhead. Upon completion of data collection, particularly at ambient temperature, the crystal is recovered. This same crystal can then be used for additional neutron experiments or to collect an X-ray dataset for joint refinement of X-ray and neutron data (see Structure Refinement).

For indexing and integration, IMAGINE uses the LAUEGEN suite of software, which was developed originally for X-ray Laue crystallography and then adapted for neutron diffraction and cylindrical detector geometries {Campbell, 1995 #284;Campbell, 1998 #1073}. Wavelength normalization is performed with Lscale {Helliwell, 1989 #1269}{Arzt, 1999 #619}. SCALA from the CCP4 suite of programs can be used to scale and merge the data {Winn, 2011 #1077}. A dedicated workstation is available to the users for on-site data reduction.

2.5. Structure refinement

Structure refinement is carried out against neutron data alone or simultaneously against both X-ray and neutron data. The latter protocol is referred to as joint refinement or X/N refinement {Afonine, 2010 #292}(Afonine, this issue). The choice of one method of refinement over the other may be influenced by the neutron dataset resolution and completeness but is ultimately the experimenter's choice. On IMAGINE, joint refinement is widely used for neutron structure refinement against data collected from partially deuterated proteins at resolutions below 2.2 Å.

Joint refinement requires that the X-ray data set be collected at the same temperature as the neutron data set. Collecting both data sets at the same temperature is essential as temperature alters aspects of the protein structure or of the crystal itself {Tilton, 1992 #1103}{Deacon, 1997 #1151}{Weik, 2010 #1095}{Fraser, 2011 #1097}{Fukuda, 2015 #1102}. While the X-ray and neutron data set would ideally be collected from the same crystal for joint refinement, the X-ray dataset is most often measured from a smaller crystal grown in the same drop or under the same crystallization conditions as the neutron crystal. X-ray data set can be collected after data collection on IMAGINE using the neutron program's ancillary facilities (section 3).

Phenix.refine is typically used to refine structures against neutron data collected on IMAGINE {Adams, 2011 #780;Adams, 2009 #1090;Afonine, 2010 #292} (Afonine et al., this issue). The phenix.refine module of the PHENIX software package is capable of refining model against both neutron data alone and joint X-ray/neutron data sets. Refinement against neutron data closely follows X-ray refinement protocols, and neutron density maps can be visualized using the program COOT {Emsley, 2004 #1128;Emsley, 2010 #622}.

3. Sample preparation and ancillary facilities

Replacing H for D in a protein crystal provides significant benefits to the neutron protein crystallography experiment {O'Dell, 2016 #1173}. The greater magnitude of the D coherent scattering length (6.671 fm) compared to H (-3.741 fm) results in greater average reflection intensities. Simultaneously, the decrease in the D incoherent scattering length compared to H dramatically reduces the isotropic background intensity. Furthermore, the D coherent scattering length is positive as is that of common atoms found in proteins while the coherent scattering length of H is negative. At the typical resolutions (1.9-2.3 Å) obtained for neutron protein crystallographic data, D substitution simplifies the analysis of neutron density maps by minimizing the number of sites where the negative coherent scattering length of H atoms leads to density cancellation.

Bulk solvent, ordered water molecules, and hydrogen atoms bound to protein oxygen, and nitrogen [(*i.e.:* titratable hydrogen atoms) can all be replaced with deuterium by preparing all reagents in deuterium oxide (D_2O) either during or after complete crystal growth. Most frequently, crystals are grown to final size in H_2O mother liquor and then subjected to H/D exchange either by vapor equilibration in capillary or soaking in an artificial H/D-exchanged mother liquor.

Titratable hydrogen atoms represent approximatively 25% of the total hydrogen atoms of any proteins. In order to exchange the remaining 75% attached to carbon atoms, proteins need to be perdeuterated during synthesis. The Bio-Deuteration Laboratory support the production of perdeuterated and 85% uniform D-labeled protein for users of the IMAGINE beamline with approved neutron beam time (https://www.ornl.gov/node/56459).

Users can take advantage of the Protein Characterization & Crystallization Laboratory which is equipped with biophysical characterization instruments, including a dynamic light scattering instrument, a circular dichroism spectropolarimeter, fluorescence microscope and

stereomicroscopes, a Gryphon crystallization robot and a Scorpion liquid dispensing robot, and 13 temperature-controlled chambers and other devices for crystallogenesis and large crystal growth. A Protein X-ray Crystallography Laboratory equipped with a Rigaku high intensity micro-focus rotating anode X-ray generator and an Eiger 6M detector is available to the users.

4. Facility access

Access to IMAGINE is granted through the HFIR and SNS User Program (https://neutrons.ornl.gov/users). Call for proposals are issued twice a year. Beam time is allocated after external scientific peer review and internal technical review. Access to the Bio-Deuteration Laboratory can be requested within the application for the neutron beam time. Access to the protein characterization and crystallization laboratories can be coordinated with the beamline scientists.

5. Highlights

Detailed highlights from the IMAGINE highlight are presented by Kovalevsky et al; this issue, Gerlits et al, this issue; Mueser et al., this issue and Ronning et al this issue.

5.1. *Neurospora Crassa* lytic polysaccharide monooxygenase 9D

Lytic polysaccharide monooxygenases (LPMOs) are copper-dependent metalloenzymes that activate molecular oxygen for the net insertion of one oxygen atom into the carbon-hydrogen bond of a glycosidic carbon in polymeric carbohydrates. LPMOs, thus, can disrupt the crystalline structure of cellulose in lignocellulosic plant biomass, and can be used in industry to enhance the efficiency of cellulose degradation by other hydrolytic enzymes for biofuels production. Therefore, detailed knowledge of the LPMO enzymatic mechanism, which requires molecular oxygen, two electrons, and two protons, is important but remains poorly understood. An examination of protonation states enabled by neutron crystallography of the LPMO enzymatic resting state and density functional theory calculations identified a role for conserved histidine (H157) in promoting oxygen activation (Fig. 2) {O'Dell, 2017 #1183;O'Dell, 2017 #1182}. The result provides a new structural description of oxygen activation by LPMOs. Fully characterizing the LPMO reaction mechanism may inform strategies for increasing the efficiency of enzymatic polysaccharide hydrolysis for applications including bioethanol production.

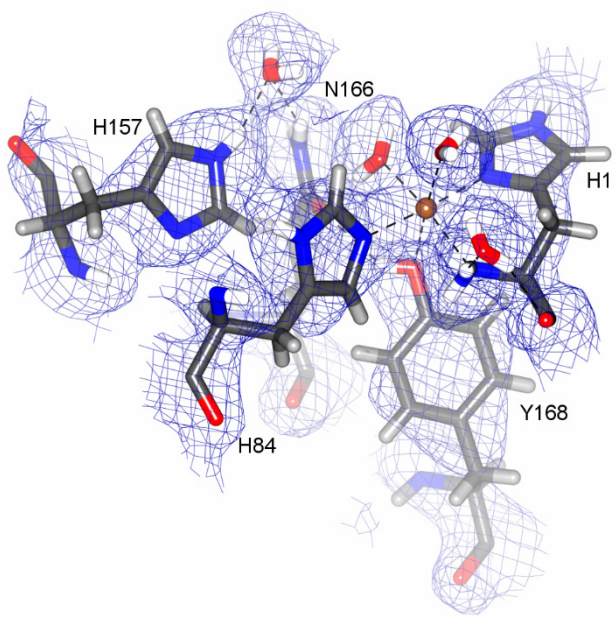

Figure 2: Active site of *Nc*LPMO9D in the enzymatic resting state (PDB 5TKI). The conformation and tautomeric state of singly-protonated H157 revealed by neutron protein crystallography was confirmed to stabilize molecular oxygen (not shown) near the LPMO active site by quantum chemical calculations. The H1 backbone amide N and carbonyl O form H-bonds with the "pocket" water molecule which has been hypothesized to participate in substrate interactions. ^{1}H atoms are shown in light grey while atoms that have undergone exchange to ^{2}H are shown in white. The copper atom is shown in brown. The blue mesh represents neutron SLD $2F_O–F_C$ map contoured at $\sigma = 1.0$.

5.3. H-RAS GTPase

The small GTPase H-RAS is a prototype for nucleotide-binding proteins that function by cycling between bound guanosine triphosphate (GTP) and guanosine diphosphate (GDP). The neutron structure of H-RAS exemplifies the uniquely rich informational content provided by a single neutron diffraction experiment {Knihtila, 2015 #1174}{Knihtila, 2019 #1366}. Previous efforts to elucidate the GTP hydrolysis mechanism of H-RAS have relied on the assumption that the γ-phosphate group of GTP bound at the active site of the enzyme would be deprotonated as is observed in solution {Cheng, 2001 #1210}. This study, however, suggests that the γ-phosphate group of the GTP ligand remains protonated at physiological pH when bound at the active site of H-RAS in the ground state (Fig. 3). The neutron structure revealed the modulation of the pK_a of the gamma-phosphate group by the H-RAS active site microenvironment and opens the possibility that the pre-catalytic state of the GTP hydrolysis reaction catalyzed by H-RAS is different than previously thought.

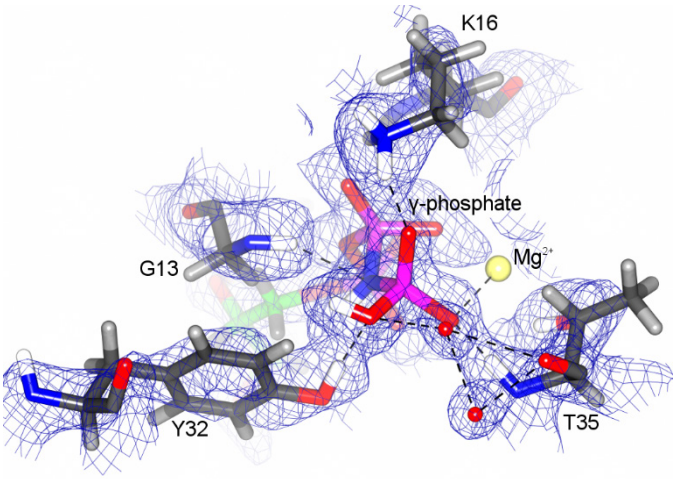

Figure 3: H-RAS in complex with GTP analogue GppNHp (PDB 4RSG). Unexpectedly, clear neutron SLD could be observed for a protonated (^{2}H) γ-phosphate in the $2F_O–F_C$ map. The deuterium atoms of the nucleophilic water (hydrogen bonded to the γ-phosphate and T35) are not visible in the density map, suggesting rotational freedom. Ligand carbon atoms are shown in green. ^{1}H atoms are shown in light grey while atoms that have undergone exchange to ^{2}H are shown in white. The blue mesh represents neutron SLD $2F_O–F_C$ map contoured at σ = 1.0.

5.4. Neutron protein crystallography at cryogenic temperature

Cold (2-10 Å) neutrons commonly used in the crystallographic experiments do not cause any observable radiation damage in protein crystals and thus most experiments are performed at room temperature. However, cryo-cooling of protein crystals in X-ray crystallography has been shown (in some cases) to provide improvements in data quality by reducing B-factors {Blakeley, 2004 #283}{Casadei, 2014 #665}. Additionally, cryo-cooling functionality opens the important possibility for freeze-trapping studies of enzymatic reaction intermediates. Until recently, cryo-cooling has been challenging for large protein crystals since the solvent must be rapidly (flash)-cooled to a vitreous glass state to avoid ice formation that disrupts the crystal lattice. Protocols for cryo-neutron protein crystallography were first developed to cool and maintain large protein crystals (1-5mm^3) at cryogenic temperatures (<15 K) using a closed cycle refrigerator{Myles, 2012 #507}. This technique requires for the crystals to be mounted in fiber loops and flash-cooled by plunging directly into liquid N_2 (77K) prior to being transferred under liquid N_2 and mounted and cooled to 15 K on the cold head of a displex cryostat. A closed-cycle refrigerator (CCR) has been recently commissioned as a standard sample environment for IMAGINE, expanding the capabilities of the instrument for neutron diffraction analysis at cryogenic temperatures. The CCR provides a constant sample temperature in the range of 4 to 450 K (Fig. 4).

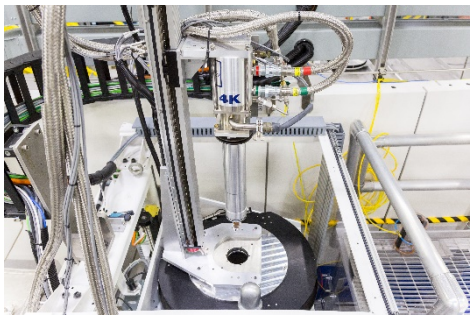

Figure 4. An automated lift moves the CCR up and down. Crystals are mounted directly onto the CCR cold finger *via* custom magnetic bases and then sealed with a heat shield (not shown) and a dome-shaped vacuum enclosure (visible at the bottom center of the photograph). A motorized vertical lift facilitates positioning of the mounted sample into the neutron beam. (Photo credit: Genevieve Martin, ORNL)

To demonstrate the suitability of the cryo-cooling set-up at IMAGINE to collect cryogenic data from protein crystals, proof-of-principle experiments have been completed in which a data set was collected on T4L lysozyme at 80K (Fig. 5){Li, 2017 #1220}. This set-up expands the capabilities of IMAGINE, allowing new scientific questions to be addressed by using the freeze-trapping technique to 'quench' kinetic processes and capture reaction intermediaries.

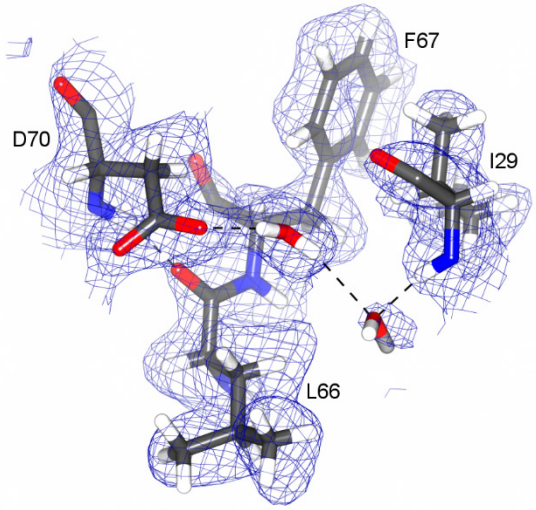

Figure 5: T4 Lysozyme "cavity 1" as observed at 80 K (PDB 5VNQ). Hydrogen atoms that were substituted with ^{2}H by covalent labeling and exchange are shown in white. The blue mesh represents neutron SLD $2F_O–F_C$ map contoured at $\sigma = 1.0$.

6. Future development

Collecting data with high completeness is complicated by the cylindrical detector geometry as well as a significant blind region arising from the curvature of the Ewald sphere at long wavelengths. Working with a single axis goniometer, crystals are typically reoriented to increase completeness by collecting data in a second crystal orientation. A miniaturized kappa goniometer head used at synchrotron beamlines has been modified and built for incorporation on IMAGINE. The Arinax MiniKappa MK3 provides an additional kappa and phi axis. This will enable data to be collected at multiple crystal settings within a single data collection run, which is expected to increase the data collection efficiency of IMAGINE. The CrystalPlan software has been adapted for IMAGINE to optimize data collection strategies using the mini-Kappa goniometer {Zikovsky, 2011 #286}. CrystalPlan uses the UB matrix determined from a short Laue geometry alignment image to predict an optimal set of crystal orientations that will maximize the completeness using a minimal number of crystal settings. These settings are then loaded and run in the instrument GUI data collection script. This will allow IMAGINE users to maximize use of available beam time per sample per experiment and increase the data collection efficiency.

Longer term, the planned 2022 replacement of the ender section located downstream of the HFIR cold source, which is known to be compromised, and upgrade of the front end of the CG-4 cold guide system will deliver a two- to four-fold increase in flux on the instrument.

7. Summary

IMAGINE is a world class neutron diffractometer that specializes in neutron protein crystallography. The instrument offers access to crystals with unit cells of up to 150 Å, complementing the capabilities of the ORNL Spallation Neutron Source MaNDi time-of-flight instrument which is optimized for larger unit cells (Coates et al., this issue). Recent upgrades have added to the capabilities of IMAGINE by providing access to data collection at variable temperatures (4K-450K), which will broaden the science that can be done on this beam line. Additionally, low temperature macromolecular neutron diffraction data can now be obtained from cryo-cooled protein crystals, making experiments with freeze-trapped intermediates in proteins possible. The unique combination of scientific and technical expertise as well as facilities for biodeuteration, crystal growth and macromolecular crystallography at ORNL provides the user community with supporting capabilities for sample preparation that help drive the productivity and development of the structural biology program at IMAGINE, allowing new scientific questions to be addressed.

Acknowledgements

This research used resources at the High Flux Isotope Reactor and Spallation Neutron Source, a DOE Office of Science User Facility operated by the Oak Ridge National Laboratory. F.M.

acknowledge support from the USDA National Institute of Food and Agriculture, Hatch project 1010523. The installation of the IMAGINE instrument was supported in part by the National Science Foundation award 0922719.

References

Arzt, S., J. W. Campbell, M. M. Harding, Q. Hao and J. R. Helliwell (1999). "LSCALE - the new normalization, scaling and absorption correction program in the Daresbury Laue software suite." Journal of Applied Crystallography **32**: 554-562.

Blakeley, M. P., A. J. Kalb, J. R. Helliwell and D. A. Myles (2004). "The 15-K neutron structure of saccharide-free concanavalin A." Proc Natl Acad Sci U S A **101**(47): 16405-16410.

Campbell, J. W. (1995). "Lauegen, an X-Windows-Based Program for the Processing of Laue X-Ray-Diffraction Data." Journal of Applied Crystallography **28**: 228-236.

Campbell, J. W., Q. Hao, M. M. Harding, N. D. Nguti and C. Wilkinson (1998). "LAUEGEN version 6.0 and INTLDM." Journal of Applied Crystallography **31**: 496-502.

Casadei, C. M., A. Gumiero, C. L. Metcalfe, E. J. Murphy, J. Basran, M. G. Concilio, S. C. Teixeira, T. E. Schrader, A. J. Fielding, A. Ostermann, M. P. Blakeley, E. L. Raven and P. C. Moody (2014). "Heme enzymes. Neutron cryo-crystallography captures the protonation state of ferryl heme in a peroxidase." Science **345**(6193): 193-197.

Cheng, H., S. Sukal, R. Callender and T. S. Leyh (2001). "gamma-phosphate protonation and pH-dependent unfolding of the Ras.GTP.Mg2+ complex: a vibrational spectroscopy study." J Biol Chem **276**(13): 9931-9935.

Coates, L., M. J. Cuneo, M. J. Frost, J. H. He, K. L. Weiss, S. J. Tomanicek, H. McFeeters, V. G. Vandavasi, P. Langan and E. B. Iverson (2015). "The Macromolecular Neutron Diffractometer MaNDi at the Spallation Neutron Source." Journal of Applied Crystallography **48**: 1302-1306.

Golden, E., L. J. Yu, F. Meilleur, M. P. Blakeley, A. P. Duff, A. Karton and A. Vrielink (2017). "An extended N-H bond, driven by a conserved second-order interaction, orients the flavin N5 orbital in cholesterol oxidase." Sci Rep **7**: 40517.

Helliwell, J. R., J. Habash, D. W. J. Cruickshank, M. M. Harding, T. J. Greenhough, J. W. Campbell, I. J. Clifton, M. Elder, P. A. Machin, M. Z. Papiz and S. Zurek (1989). "The Recording and Analysis of Synchrotron X-Radiation Laue Diffraction Photographs." Journal of Applied Crystallography **22**: 483-497.

Knihtila, R., G. Holzapfel, K. Weiss, F. Meilleur and C. Mattos (2015). "Neutron Crystal Structure of RAS GTPase Puts in Question the Protonation State of the GTP gamma-Phosphate." Journal of Biological Chemistry **290**(52): 31025-31036.

Li, L., S. Shukla, F. Meilleur, R. F. Standaert, J. Pierce, D. A. A. Myles and M. J. Cuneo (2017). "Neutron crystallographic studies of T4 lysozyme at cryogenic temperature." Protein Sci **26**(10): 2098-2104.

Myles, D. A. A., F. Dauvergne, M. P. Blakeley and F. Meilleur (2012). "Neutron protein crystallography at ultra-low (< 15 K) temperatures." Journal of Applied Crystallography **45**: 686-692.

O'Dell, W. B. and (2017). Structural Investigations of the Fungal Lytic Polysaccharide Monooxygenase Reaction Mechanism using X-ray and Neutron Protein Crystallography. Doctor of Philosophy, North carolina State University.

O'Dell, W. B., P. K. Agarwal and F. Meilleur (2017). "Oxygen Activation at the Active Site of a Fungal Lytic Polysaccharide Monooxygenase." Angew Chem Int Ed Engl **56**(3): 767-770.

O'Dell, W. B., P. D. Swartz, K. L. Weiss and F. Meilleur (2017). "Crystallization of a fungal lytic polysaccharide monooxygenase expressed from glycoengineered Pichia pastoris for X-ray and neutron diffraction." Acta Crystallogr F Struct Biol Commun **73**(Pt 2): 70-78.
Winn, M. D., C. C. Ballard, K. D. Cowtan, E. J. Dodson, P. Emsley, P. R. Evans, R. M. Keegan, E. B. Krissinel, A. G. W. Leslie, A. McCoy, S. J. McNicholas, G. N. Murshudov, N. S. Pannu, E. A. Potterton, H. R. Powell, R. J. Read, A. Vagin and K. S. Wilson (2011). "Overview of the CCP4 suite and current developments." Acta Crystallographica Section D-Biological Crystallography **67**: 235-242.
Zikovsky, J., P. F. Peterson, X. P. Wang, M. Frost and C. Hoffmann (2011). "CrystalPlan: an experiment-planning tool for crystallography." Journal of Applied Crystallography **44**(2): 418-423.